SCIENTIFIC REPORTS

OPEN

SUBJECT AREAS:
SOLAR CELLS
ELECTRONIC DEVICES
ENERGY TRANSFER
RENEWABLE ENERGY

Received
7 June 2013

Accepted
25 July 2013

Published
15 August 2013

Correspondence and requests for materials should be addressed to J.-H.Y. (junho.yum@epfl.ch)

Blue-Coloured Highly Efficient Dye-Sensitized Solar Cells by Implementing the Diketopyrrolopyrrole Chromophore

Jun-Ho Yum[1], Thomas W. Holcombe[1], Yongjoo Kim[1,2], Kasparas Rakstys[1,3], Thomas Moehl[1], Joel Teuscher[1], Jared H. Delcamp[1,4], Mohammed K. Nazeeruddin[1] & Michael Grätzel[1]

[1]Insitute of chemical sciences and engineering, École Polytechnique Fédérale de Lausanne, Station 6, 1015-Lausanne, Switzerland, [2]R & D Center DSC Team, Dongjin Semichem Co., LTD. 445-935 Hwasung, South Korea, [3]Department of Organic Chemistry, Kaunas University of Technology, Radvilenu plentas 19, LT50254, Kaunas, Lithuania, [4]Department of Chemistry and Biochemistry, University of Mississippi, University, MS 38677, USA.

The paradigm shift in dye sensitized solar cells (DSCs) – towards donor- π bridge-acceptor (D-π-A) dyes – increases the performances of DSCs and challenges established design principles. Framed by this shifting landscape, a series of four diketopyrrolopyrrole (DPP)-based sensitizers utilizing the donor-*chromophore*-anchor (D-*C*-A) motif were investigated computationally, spectroscopically, and fabricated by systematic evaluation of finished photovoltaic cells. In all cases, the $[Co(bpy)_3]^{3+/2+}$ redox-shuttle afforded superior performance compared to I_3^-/I^-. Aesthetically, careful molecular engineering of the DPP chromophore yielded the first example of a high-performance blue DSC – a challenge unmet since the inception of this photovoltaic technology: DPP17 yields over 10% power conversion efficiency (PCE) with the $[Co(bpy)_3]^{3+/2+}$ electrolyte at full AM 1.5 G simulated sun light.

Dye-sensitized solar cells (DSCs) are an attractive alternative energy source, with the potential for high-efficiency and low-cost power production[1,2]. Choosing the appropriate nanostructured metal oxide (most commonly TiO_2), sensitizer, and redox shuttle offers control over aesthetic properties such as transparency and colour, as well as performance properties such as the attainable output voltage and current density[3]. One of the most critical components within a DSC is the sensitizer, as this constituent not only determines the light-harvesting properties of the DSC, but it also mediates the interaction between the redox shuttle and the TiO_2[4,5]. State of the art DSCs now rely on the donor-π-bridge-acceptor (D-π-A) motif and have recently achieved greater than 10% power conversion efficiency (PCE)[6–10]. However, only the zinc-porphyrin (ZnP)[6,8] and ruthenium classes of sensitizers[11,12] consistently achieve greater than 10% PCE, limiting synthetic versatility and industrial compatibility. However, one exceptional example was reported by utilizing the cyclopentadithiophene-bridged donor-acceptor dye (Y123) and the $[Co(bpy\text{-}pz)_2]^{3+/2+}$ redox shuttle to yield an incredible open circuit voltage (V_{oc}) of over 1,000 mV and a 10.08% PCE[10]. By looking to industrial pigment technology, we have started to develop the synthetically/industrially accessible, low-bandgap chromophore diketopyrrolopyrrole (DPP) for DSC applications.

Herein, we describe the design and synthesis of high-performance, blue-coloured DPP-based sensitizers. In addition to PCE, the aesthetic properties of solar cells are critical for public acceptance, particularly for indoor applications. There exist very few blue sensitizers, and none possess high efficiency. For instance, squaraine sensitizers yield blue coloured devices, but the PCEs achieved are below 5.5%, owing to their narrow absorption in the red/near-infrared (NIR) region and low open circuit voltage (V_{oc})[13–18]; enhanced PCEs of around 7% have been achieved through additional absorption in the high energy region below 550 nm[19,20]. Furthermore, absorption beyond 700 nm is not straightforwardly achieved utilizing the typical, D-π-A, metal-free organic sensitizer embodiment.

The DPP moiety has enjoyed widespread use in materials technology, from car-paint pigments[21] to polymer and small molecule organic photovoltaics[22,23]. However, DPP-based sensitizers have thus far exhibited limited use in DSCs[24–29]. This may be due to an incomplete understanding of how to molecularly engineer this

promising chromophore into a suitable DSC sensitizer, utilizing the donor-*chromophore*-anchor (D-C-A) motif. Towards elucidating the potential of DPP in DSC devices, we recently completed two structure-property relationship studies: the first examined the symmetric thienyl-DPP (ThDPP) core[30] and the second exposed the benefits of an asymmetric phenyl-DPP-thienyl (PhDPPTh) core[31]. We discovered that the asymmetric DPP core (DPP07) enhanced device performance, despite a loss in absorption breadth compared the symmetrical analogue. Indeed, the maximum absorbance of DPP07 was ~80 nm blue-shifted compared to the symmetric DPP03 sensitizer. Nevertheless, DPP07 yielded 7.8% PCE compared to the 4.9% PCE achieved by DPP03. In order to improve upon the DPP07 design, here we attempt to recover the red light response by further engineering the bridge conjugation and modulating the donor group; this structure-property relationship was investigated in the context of both I_3^-/I^- and $Co[(bpy)_3]^{3+/2+}$-based electrolyte devices. By rational design, DPP17 yields the first example of a high-performance blue DSC, over 10% PCE, with the $[Co(bpy)_3]^{3+/2+}$electrolyte at full AM 1.5 G simulated sun light – a challenge unmet since the inception of this photovoltaic technology. Spectroscopic, electrochemical, and quantum chemical investigations of these sensitizers were undertaken to understand how structural modifications to the DPP chromophore affect the colour and performance properties of finished DSC devices.

Results

Compared to the phenylcyanoacrylic acid anchor of DPP07[31], here the furanylcyanoacrylic acid anchor is employed for all the sensitizers, aiming to increase the influence of the cyanoacrylic acid acceptor group. To further maximize the donor-acceptor effect on the DPP chromophore, the electron donating amine was installed on the thiophene unit of the asymmetric PhDPPTh structure, ensuring planarity and facile electronic communication to the relatively electron deficient bicyclic double lactam core. The standard *p*-hexyloxytriphenyl amine donor was employed as well as indoline-based donors with varying steric bulk. When implementing the cobalt redox shuttle, suppressing counter-productive charge carrier recombination between the electrolyte and the TiO_2 surface is critical to realizing maximum device performance; bulky alkoxy moieties have recently been shown to alleviate this loss mechanism[4,5]. Here, we employ indoline donors with increasing alkoxy bulk, from DPP14 to DPP15 to DPP17 (see molecular structures in Figure 1a).

The optical and electrochemical properties of all dyes are summarized in Table 1. Replacing the anchoring phenyl ring of DPP07 with the furan ring of DPP13 provides a ~20 nm red-shift in the charge-transfer (CT) light absorption band in combination with increased intensity of the CT band compared to the higher energy band. Additionally, a bathochromic shift of the higher energy band is observed as shown in Figure 1b, as discussed with the computational results below. By employing strongly electron donating indoline groups in DPP14, DPP15, and DPP17 a further ~10 nm red-shift in the low-energy excitation compared to DPP13 was observed. It is worth noting that the slightly extended conjugation of the indoline donor on DPP17 drives the high-energy absorption into the visible region, ~15 nm red-shifted compared to DPP14 and DPP15, and dramatically increases the molar extinction coefficient in this region up to ~65,000 M^{-1} cm^{-1}. This red-shifted high-energy absorption peak increases the light harvesting efficiency overall, leading to enhanced photocurrent. Importantly, all these DPP sensitizers absorb 400 nm light, while exhibiting relatively less absorption in the 450–500 nm range, manifesting the observed blue colour.

Given that density functional theory (DFT) has become a powerful tool for the materials chemist[32], we set out to further understand the molecular properties of this series with DFT-based quantum chemical calculations. Structurally similar compounds, Pechmann dyes, were recently investigated computationally[33], and some of the functionals and basis sets that were determined to be the best for that study were adopted here. Particularly, an extensive study concerning

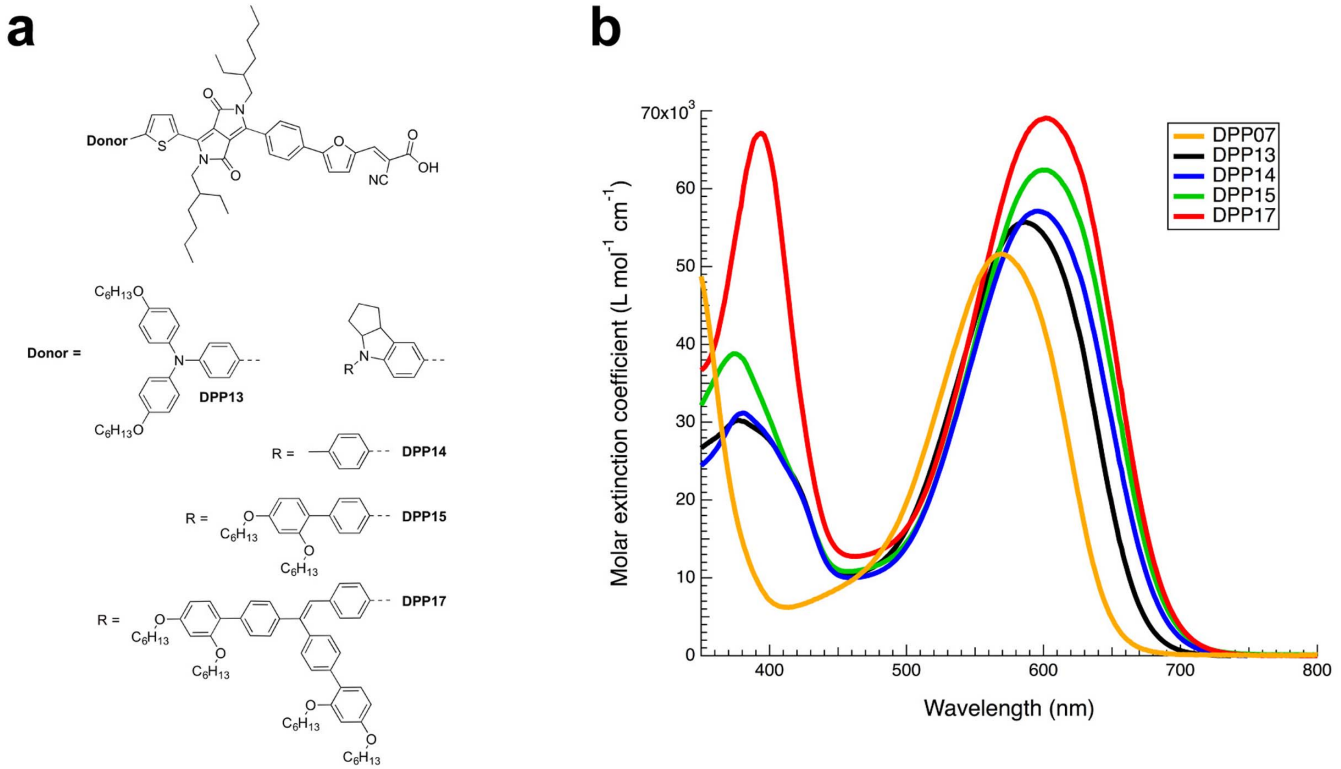

Figure 1 | Molecular structures and optical properties. (a) Molecular structures of the investigated sensitizers. (b) All UV-Vis spectra DPP07 (orange), DPP13 (black), DPP14 (blue), DPP15 (green), and DPP17 (red) measured in THF (~2×10^{-5} M).

Table 1 | Optical and electrochemical properties of dyes. [a]Absorbances of the dyes with $\sim 2 \times 10^{-5}$ M concentration in THF solution. [b]The ground-state oxidation potential of the dyes was measured under the following conditions: electrolyte, 0.1 M tetra-*n*-butylammonium hexafluorophosphate in dimethylformamide; electrode, Platinum counter and reference electrodes were used with a glassy carbon working electrode. Potentials measured vs. Fc^+/Fc were converted to NHE by addition of +0.69 V[39]. [c]Optical transition energy, estimated from the onset of the absorption. [d]Excited-state oxidation potential energies *vs.* NHE estimated from the ground-state oxidation potential (E_{Ox}), by subtracting the bandgap (E_g^{opt})

Dye	ε (M^{-1} cm^{-1}) [Abs_{max} (nm)][a]	$E_{(S+/S)}$ (V)[b]	$E_{(S-/S)}$ (V)[b]	E_g^{opt} (eV)[c]	$E_{(S+/S^*)}$ (V)[d]
DPP13	30,300 (377)/55,700 (587)	0.99	−0.98	1.85	−0.86
DPP14	31,200 (380)/57,100 (596)	0.94	−0.98	1.81	−0.87
DPP15	38,800 (374)/62,400 (600)	0.94	−0.96	1.80	−0.86
DPP17	67,000 (393)/69,000 (602)	0.98	−0.99	1.80	−0.82

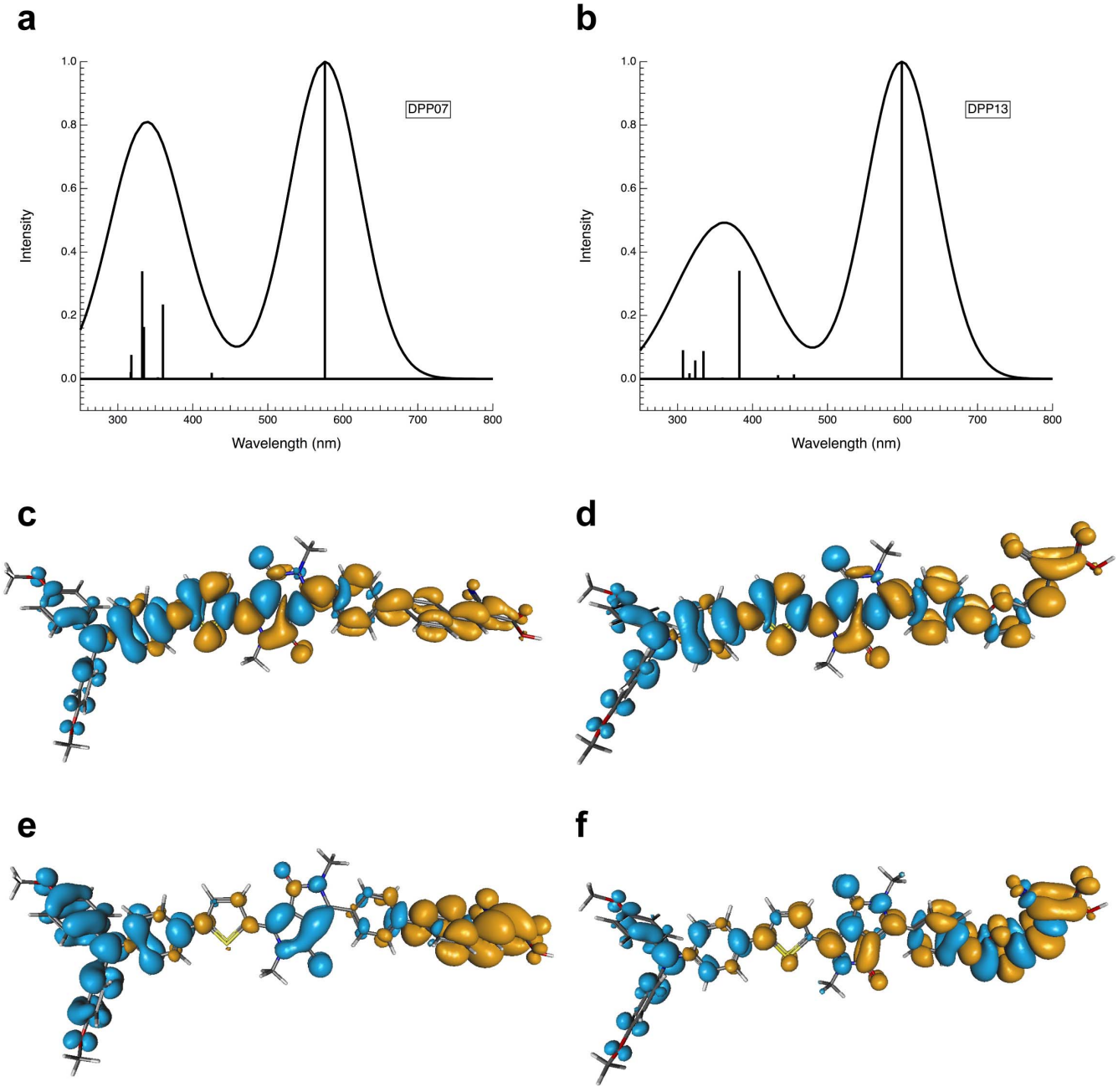

Figure 2 | TD-DFT calculation result of DPP07 and DPP13. The calculated absorption spectra for (a) DPP07 and (b) DPP13, showing the electronic transitions that make up the spectrum. A contour plot of the transition density difference ($\rho S_1 - \rho S_0$), where blue symbolizes the positive (hole) contribution while gold represents (negative) electron contribution, of the lowest energy excitation for DPP07 (c) and DPP13 (d), and of the 4th lowest energy excitation for DPP07 (e) and DPP13 (f).

the relative percentage Hartree-Fock component in the time dependent (TD)-DFT analysis was performed, and the BMK[34] functional was found to be optimal. This was confirmed by us to be true for the DPP class of compounds (see SI).

The ground state geometry was optimized with the M06[35] functional and 6-31 G* basis set with a methylene chloride SMD[36] solvent model. The TD-DFT was performed on these optimized geometries with the BMK functional and the DGDZVP[37,38] basis set to provide the first ten lowest energy excited states. For all dyes, representative HOMO and LUMO orbitals, as well as experimental and calculated UV-Vis spectra are presented in Figures S2 and S3. The charge-transfer absorption band is modelled extremely accurately, while the higher energy absorption band is slightly blue-shifted and slightly lower in intensity than established empirically. This is likely an outcome of the inability to perfectly match the correct functional (and corresponding Hartree-Fock percentage) for both excitation transitions. However, the model does still accurately predict the reduced intensity and bathochromic shift of the higher energy response into the visible for DPP13 compared to our benchmark sensitizer DPP07. Analysing the difference density for this excitation, the 4th lowest energy transition, indicates that the planarity of the furan ring with the DPP bridge is what lowers this excitation energy; increased electron-hole delocalisation in this high energy excitation indicates that the electron withdrawing cyanoacrylic acid is more effectively conjugated with the rest of the molecule (see Figure 2e and 2f). Additionally, the HOMO and LUMO pictures clearly evince vectorial electron motion, from the donor to the acceptor, across the chromophoric DPP bridge (Figure S3).

Electrochemical features were characterized with differential pulse voltammetry measurements. The ground-state oxidation potentials ($E_{(S+/S)}$) were determined to be 0.25–0.30 V *vs.* Fc^+/Fc, corresponding to 0.94–0.99 V *vs.* normal hydrogen electrode (NHE). Given the HOMO-LUMO bandgap (E_g^{opt}) taken from the onset of the absorbance, 1.80 ~ 1.85 eV, the corresponding excited-state oxidation potentials ($E_{(S+/S^*)}$) are calculated to be −0.82 ~ −0.87 V *vs.* NHE (see all details in Table 1). This provides ample thermodynamic driving force for both electron injection into TiO_2, and reduction of the dye cation by the redox shuttle I_3^-/I^- or $[Co(bpy)_3]^{3+/2+}$.

Table 2 | Comparison of photovoltaic characteristics of DSCs sensitized by DPP07, DPP13, DPP14, DPP15, and DPP17 as electrolyte. A double layer consisting of a ~3.5 μm transparent film composed of nanocrystalline anatase particles and a ~4 μm scattering layer (of 400 nm, CCIC, Japan) was employed for all devices except DPP07 taken from a previous study[31]. EL_I (iodine based electrolyte) contains 0.6 M 1,3-dimethylimidazolium iodide, 0.03 M I_2, 0.05 M LiI, 0.05 M guanidinium thiocyanate, and 0.25 M 4-*tert*-butylpyridine in 15/85 (v/v) mixture of valeronitrile and acetonitrile. EL_Co (cobalt tris-bpy based electrolyte) contains 0.22 M Co(II), 0.05 M Co(III), 0.1 M $LiClO_4$, and 0.2 M 4-*tert*-butylpyridine in acetonitrile

Dye	Redox	J_{sc} (mA cm^{-2})	V_{oc} (mV)	FF	PCE (%)
DPP07	EL_I[(a)]	15.6	680	0.73	7.67
	EL_Co	15.1	766	0.76	8.79
DPP13	EL_I	16.2	705	0.67	7.60
	EL_Co	15.6	743	0.78	8.97
DPP14	EL_I	16.6	680	0.68	7.73
	EL_Co	15.2	716	0.76	8.23
DPP15	EL_I	16.9	684	0.65	7.44
	EL_Co	17.6	745	0.75	9.81
DPP17	EL_I	16.3	700	0.63	7.13
	EL_Co	17.9	761	0.74	10.1

(a) Data taken from reference[31].

All sensitizers were tested in DSCs with both the I_3^-/I^- (coded EL_I) and the cobalt tris-bipyridyl complex $[Co(bpy)_3]^{3+/2+}$ (coded EL_Co) electrolytes. The devices employing $[Co(bpy)_3]^{3+/2+}$ electrolyte outperformed I_3^-/I^- based devices, as higher open circuit voltage (V_{oc}) and fill factor (FF) provided significant performance enhancement (Table 2). The devices employing EL_I generated short circuit current densities of 16–17 mA cm^{-1} and overall PCEs greater than 7% (see output characteristics in Table 2 and Figure 3). Importantly, the enhanced absorption properties of DPP13 compared to the benchmark sensitizer DPP07 were reflected in the incident photon-to-electron conversion efficiency (IPCE), leading to the higher current and confirming the utility of the furanylcyanoacrylic acid anchor (see Figure 3). The IPCEs of DPP14 and 15 exceeded 60% over most of visible light region from 400 to 700 nm, with a maximum of ~80% at around 570 nm – the lowest values being between 400–500 nm. Gratifyingly, DPP17 exhibited better performance in this region, while maintaining a vivid blue colour. Overall, the best PCE for the EL_I was obtained with DPP14 at 7.73%. The DPP17 achieved over 10% PCE, followed by DPP15 (9.81%), DPP13 (8.97%), DPP07 (8.69%), and DPP14 (8.23%). Enhanced photocurrent led to a higher PCE for DPP13 compared to DPP07, despite of a small loss in V_{oc}. Implementing the smallest indoline-based donor in DPP14 yielded a PCE of 8.23%, which was mainly due to a loss in the V_{oc} compared to DPP07 and DPP13.

The utility of the 2,4-bisalkoxybiphenyl moiety on the donor of typical D-π-A organic dyes has proven effective towards realizing high V_{oc} with the cobalt-based redox shuttle[4,5]. We envisaged the same effect applies for the donor-*chromophore*-anchor (D-*C*-A) DPP dyes and the indoline-based donor. Accordingly, the two dyes with bulky N-substituted indolines (DPP15 and DPP17) provided enhanced V_{oc} over DPP14. The photocurrents for DPP15 and DPP17 devices, astonishingly, increased to almost 18 mA cm^{-2} and these increases were reflected in the IPCEs (Figure 3). All IPCEs of DPP dyes exceeded 60% over most of the visible light region from 400 to 700 nm, with a maximum of over 70% at around 570 nm. Gratifyingly, DPP17 exhibited the best performance over the whole visible light region with a maximum of 86% also at 570 nm. DPP17 is the highest performing blue coloured dye, to the best of our knowledge (see colours of all dyes in THF and on a ~3 μm transparent TiO_2 film in Figure 4), and the aesthetic advantages of a blue sensitizer are much more attractive with such strong performance. Notably, DPP17 achieved over 9% PCE on only ~3.2 μm thick transparent TiO_2 films, allowing for the development of blue, semi-transparent solar cells for building Integration PV applications.

The fill factor values in cobalt-based devices also showed pronounced improvement compared to EL_I-based devices. While Pt is known as the best electrolyte regeneration catalyst for the I_3^-/I^- based electrolyte, a carbonaceous type catalyst as used in this study is generally known to outperform Pt in the cobalt redox system, owing to the low charge transfer resistance particularly for the cobalt[40–42]. However, the fill factor in DPP dyes based devices with the EL_I electrolyte were relatively low with the Pt counter electrode due to the occurrence of an s-shaped IV curve, which was most pronounced in the DPP17 device. To clarify the origin of the difference in the fill factor, we first performed transient absorption spectroscopy (TAS) at open circuit condition and electrochemical impedance spectroscopy (EIS) measurements obtained at different bias voltage under dark and illumination for the DPP17 device.

The regeneration rates estimated from TAS are 95% for DPP17 (see Figure S4): In inert solvent, acetonitrile:valeronitrile, the oxidized dye possesses a lifetime of t_{rec} = 208 μs; upon addition of electrolyte, regeneration of the oxidized dye by the redox shuttle is observed with the monoexponential time constant t_{reg} = 11 μs (EL_Co), yielding 95% regeneration efficiency, assuming first order kinetic laws for charge recombination and dye regeneration reactions[43]. A slightly

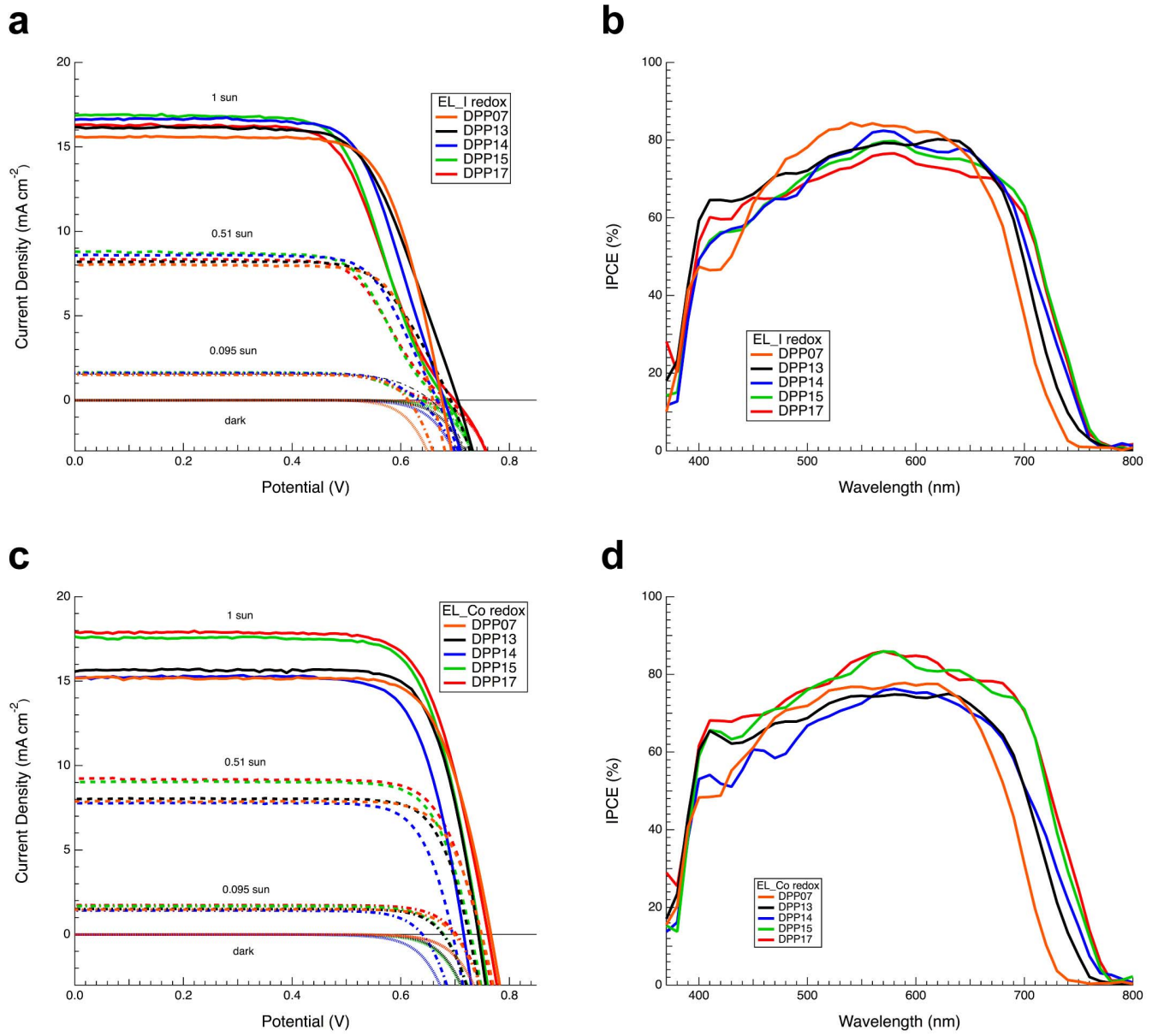

Figure 3 | Photovoltaic performance DPP dye-sensitized solar cells with EL_I and EL_Co electrolyte. (a, b) IV characteristics and IPCEs of DPP07 (orange lines), DPP13 (black lines), DPP14 (blue lines), DPP15 (green lines), and DPP17 (red lines) sensitized solar cells with EL_I. (c, d) IV characteristics and IPCEs of DPP07 (orange line), DPP13 (black line), DPP14 (blue line), DPP15 (green line), and DPP17 (red line) sensitized solar cells with EL_Co. All detailed performances as a function of light intensity are described in Table S1.

lower lifetime of the oxidized dye can be observed in the case of the EL_I.

The EIS analysis is presented in the Figure 5. First, we examined the real part of the Warburg diffusion resistance ($R_{Electrolyte}$), the counter electrode resistance (R_{CE}), and the contact and substrate resistance (R_S), which determines the total series resistance ($R_{All,series} = R_S + R_{CE} + R_{Electrolyte}$) (see Figure 5a). It is noted that the series resistances in both types of devices show similar values and tendencies. The resistance R_S in case of the cobalt based device shows a lower value probably due to the gold on top of the FTO, reducing the sheet resistance of this electrode. A low FF is generally ascribed to high sheet resistance and/or a high series resistance[44,45], however, neither is significantly impacted by the different electrolyte or catalyst. It is therefore obvious that the series resistance of the EL_I based devices is not the cause of the low fill factor. Figure 5b shows the charge recombination and transport resistance as well as the chemical capacitance of the TiO_2. The recombination resistance at the TiO_2/electrolyte interface under illumination shows a reduction from about 400 mV forward bias on. It is interesting to observe the unusually low recombination resistance in the EL_I redox system compared to other iodine based DSCs and how it increases again from about 600 mV on to 700 mV (after which it drops again). To better understand the evolution of the electron lifetime ($\tau_e = R_{CT} * C_{Chem}$) and electron transport time ($\tau_{trans} = R_{trans} * C_{Chem}$) with raising Fermi level, we plotted τ_e and τ_{trans} against the same charge density inside the TiO_2 (Figure 5c); similar DOS should imply similar E_F of the TiO_2. An unusual rise in τ_e is clearly observed at higher E_F, DOS = 1.5×10^{19} cm^{-3} for the devices made with EL_I electrolyte, while the τ_{trans}'s are almost identical in the range of error in both electrolyte systems (which circumstantiates the usage of the DOS as indirect measure of the E_F). This is an unexpected behaviour especially in comparison with the evolution of the electron lifetime with other organic dye/cobalt electrolyte systems[10] (see Figure S5) and led clearly to the loss in fill factor. From the EIS measurements it seems

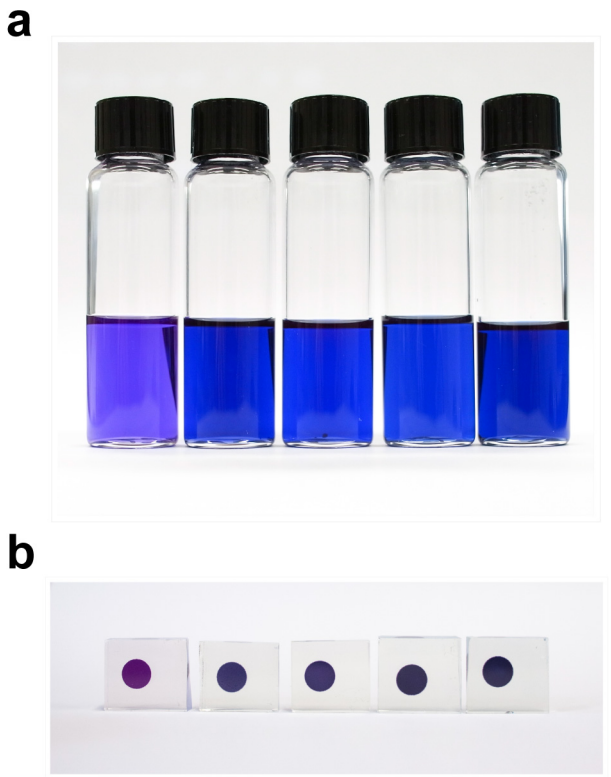

Figure 4 | Colour of DPP07, 13, 14, 15, and 17 (from left to right). (a) DPP dyes are dissolved in THF solution (0.025 mM) and (b) DPP dyes are adsorbed on 3 μm thick TiO_2 film.

that the electron lifetime increases as soon as sufficient dark current is channelled over the mesoporous TiO_2. To elucidate the origin of this result, more in-depth studies will be necessary which extend beyond the scope of this rapid communication.

Discussion

We increased the red light response of asymmetric DPP dyes by judicious engineering of the sensitizer molecular structure. Replacing the phenylcyanoacrylic acid of DPP07 with the furanyl-cyanoacrylic acid anchor of DPP13 is confirmed to enhance absorption properties and the incident photon-to-electron conversion efficiency. By employing strongly electron donating indoline groups in DPP14, DPP15, and DPP17 a further ~10 nm red-shift in the low-energy absorption band compared to DPP13 was achieved and in particular the slightly extended conjugation of the indoline donor on DPP17 drove the high-energy absorption into the visible region. These sensitizers provided the highest performance for DPP-based sensitizers, to date. Maximum power conversion efficiencies of 8–10% were achieved with the cobalt redox system, in particular over 9% for DPP15 and greater than 10% for DPP17. Incorporating 2,4-bishexyloxybiphenyl steric bulk on the donors of DPP15 and DPP17 provided enhanced V_{oc} and PCE for these sensitizers compared to DPP14. In fact, DPP15 and DPP17 firmly establish DPP-based dyes as one of the highest classes of organic dyes known in DSCs. Moreover, all dyes show an aesthetically pleasing blue colour both in solution and on the TiO_2 film. Future rational design for the DPP dye should be towards increasing output voltage, leading to further increased power conversion efficiency.

Methods

Synthetic Methods and Materials. All detailed synthetic procedures are described in SI.

DSC fabrication. DSCs were prepared using a previously reported procedure[30,31]. In brief, the TiO_2 transparent electrodes composed of ~20 nm anatase resulting in ~30 nm pore on fluorine doped thin oxide (FTO, 4 mm thickness, 10 ohms/sq, Nippon Sheet Glass, Japan) conducting glass were controlled to get a desired thickness, e.g. ~3.5 μm. A 4 ~ 5 μm scattering layer (400 nm, CCIC, HPW-400) was printed on the top of the transparent layer to increase light path length by scattering. The TiO_2 electrodes were immersed into a 0.025 mM solution of a dye with 1.25 mM (DPP07, DPP13) or 2.5 mM (DPP14, 15, 17) of 3α,7α-dihydroxy-5β-cholic acid (chenodeoxycholic acid) in 4-*tert*-butanol/acetonitrile mixture (1 : 1 v/v) and kept for 15 h at room temperature. Two electrolyte were applied: EL_I (iodine based electrolyte contains 0.6 M 1,3-dimethylimidazolium iodide, 0.03 M I_2, 0.05 M LiI, 0.05 M guanidinium thiocyanate, and 0.25 M 4-*tert*-butylpyridine in 15/85 (v/v) mixture of valeronitrile and acetonitrile) and EL_Co (cobalt tris-bpy based electrolyte contains 0.22 M Co(II), 0.05 M Co(III), 0.1 M $LiClO_4$, and 0.2 M 4-*tert*-butylpyridine in acetonitrile). As for the counter electrode, a platinized counter electrode and carbonaceous catalyst FTO (TEC 15 ohms/sq, Pilkington) were used for EL_I and EL_Co electrolyte system, respectively. The carbonaceous typed catalyst has been in general known to perform better than Pt owing to the low charge transfer resistance particularly for the cobalt redox system[40–42]. The dye-adsorbed TiO_2 electrode and the counter electrode were assembled into a sealed sandwich type cell with a gap of a hot-melt ionomer film, Surlyn (25 μm, Du-Pont).

DSC characterization. A 450 W xenon light source (Oriel, USA) was used to characterize the solar cells. The spectral output of the lamp was matched in the region of 350–750 nm with the aid of a Schott K113 Tempax sunlight filter (Präzisions Glas & Optik GmbH, Germany) so as to reduce the mismatch between the simulated and true solar spectra to less than 4%. The current–voltage characteristics of the cell under

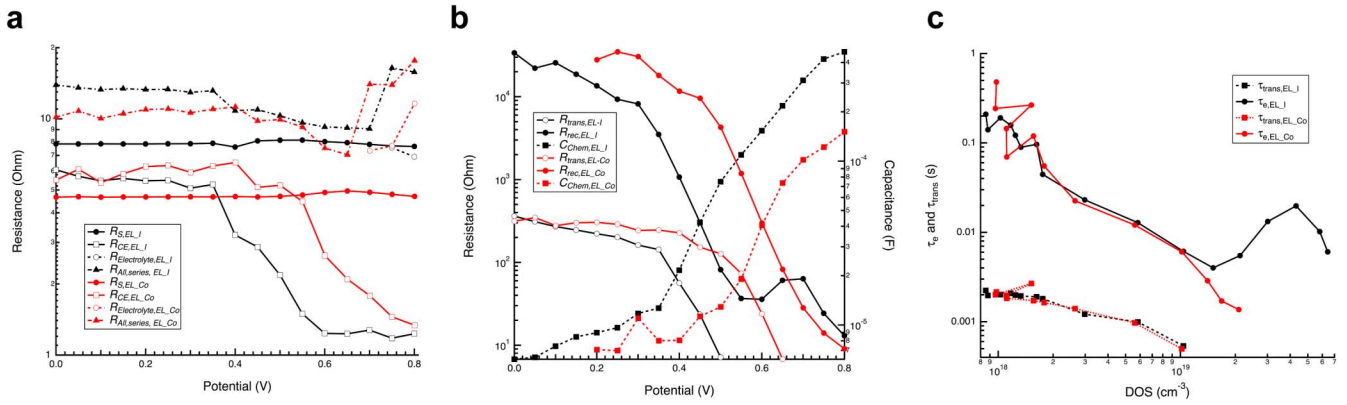

Figure 5 | EIS result of DPP17 device. (a) The contact and substrate resistance (R_S, closed circles), the charge transfer resistance at counter electrode (R_{CE}, open squares), the Warburg diffusion resistance ($R_{Electrolyte}$, dotted line with open circles), the total series resistance ($R_{All,series}$, dash dotted line with closed triangles) of EL_I (black lines) and EL_Co (red lines) systems. (b) Charge transport resistance, (R_{trans}, open circles), recombination resistance, (R_{rec}, closed circles), and chemical capacitance of the TiO_2, (C_{Chem}, closed squares with dashed line) of EL_I (black lines) and EL_Co (red lines) based device under illumination of ~1 sun by LED plotted against the IR drop corrected potential. (c) Electron lifetime (τ_e, solid) and transport time (τ_{trans}, dotted line) plotted against the DOS.

these conditions were obtained by applying external potential bias to the cell and measuring the generated photocurrent with a Keithley model 2400 digital source meter (Keithley, USA). For IPCE measurement, a modulated light intensity data acquisition system was used to control the Incident Photon-to-Current conversion Efficiency (IPCE) measurement. The modulation frequency was about 1 Hz. Light from a 300 W Xenon lamp (ILC Technology, USA) was focused through a computer controlled Gemini-180 double monochromator (Jobin Yvon Ltd., UK) onto the photovoltaic cell under test. A white light bias was used to bring the total light intensity on the device under test closer to operating conditions. The devices were masked with a black metal aperture to attain an illuminated active area of 0.2 cm^2. Photovoltage transients were observed by using a pump pulse generated by 4 red light emitting diodes controlled by a fast solid-state switch with a white light bias. The pulse of red light with widths of 50 ms was incident on the photoanode side of the cell, and its intensity was controlled to keep a suitably low level to generate the exponential voltage decay where the charge recombination rate constants are obtained directly from the exponential decay rate[46]. A white bias light, also incident on the same side of the device, was supplied by white diodes. Small perturbation transient photocurrent measurements were performed in a similar manner to the open-circuit voltage decay measurement.

Transient absorbance spectroscopy. An optical parametric oscillator (OPO, GWU-350) is pumped by a Continuum Powerlite 7030 frequency-tripled Q-switched Nd:YAG laser (λ = 355 nm, 20 Hz repetition rate). The output of the OPO (5 ns FWHM) is tuned at 600 nm. The beam fluence is kept low, typically below 50 $\mu J\ cm^{-2}$ at the sample, especially for recombination dynamics. This corresponds to the injection of less than an electron per nanoparticle, on average. A Xenon arc lamp, filtered through a monochromator and various filters, constitutes the probe beam. It is focused onto the sample and then collected in a second monochromator at 800 nm and detected by a fast photomultiplier tube (R9110, Hamamatsu) supplied with −750 V. The induced transient voltage signal is then recorded with an oscilloscope (Tektronix). Typical acquisition requires averaging of 1000 laser shots to obtain satisfactory signal to noise ratio and a Savitsky-Golay filter to smooth the data.

Electrochemical impedance spectroscopy. Electrochemical impedance spectroscopy (EIS) was performed by a Bio-Logic SP300 (France) in a frequency range between 7 MHz and 0.1 Hz for forward bias potentials between 0 to V_{oc} (with a 10 mV sinusoidal AC perturbation) in 50 mV steps. The resulting impedance spectra were analysed with ZView software (Scribner Associate Inc) on the basis of the two-channel transmission line model[47]. If results of the EIS are plotted against IR drop corrected potential this is mentioned in the figure caption.

1. O'Regan, B. & Grätzel, M. A Low-Cost, High-Efficiency Solar-Cell Based on Dye-Sensitized Colloidal TiO_2 Films. *Nature* **353**, 737–740 (1991).
2. Hardin, B. E., Snaith, H. J. & McGehee, M. D. The renaissance of dye-sensitized solar cells. *Nat. Photonics* **6**, 162–169 (2012).
3. Hagfeldt, A., Boschloo, G., Sun, L. C., Kloo, L. & Pettersson, H. Dye-Sensitized Solar Cells. *Chem. Rev.* **110**, 6595–6663 (2010).
4. Feldt, S. M. *et al.* Design of Organic Dyes and Cobalt Polypyridine Redox Mediators for High-Efficiency Dye-Sensitized Solar Cells. *J. Am. Chem. Soc.* **132**, 16714–16724 (2010).
5. Gao, P. *et al.* Facile synthesis of a bulky BPTPA donor group suitable for cobalt electrolyte based dye sensitized solar cells. *J. Mater. Chem. A* **1**, 5535–5544 (2013).
6. Bessho, T., Zakeeruddin, S. M., Yeh, C.-Y., Diau, E. W.-G. & Grätzel, M. Highly Efficient Mesoscopic Dye-Sensitized Solar Cells Based on Donor–Acceptor-Substituted Porphyrins. *Angew. Chem., Inter. Ed.* **49**, 6646–6649 (2010).
7. Zeng, W. D. *et al.* Efficient Dye-Sensitized Solar Cells with an Organic Photosensitizer Featuring Orderly Conjugated Ethylenedioxythiophene and Dithienosilole Blocks. *Chem. Mater.* **22**, 1915–1925 (2010).
8. Yella, A. *et al.* Porphyrin-Sensitized Solar Cells with Cobalt (II/III)-Based Redox Electrolyte Exceed 12 Percent Efficiency. *Science* **334**, 629–634 (2011).
9. Cao, Y. M. *et al.* Modulating the assembly of organic dye molecules on titania nanocrystals via alkyl chain elongation for efficient mesoscopic cobalt solar cells. *Phys. Chem. Chem. Phys.* **14**, 8282–8286 (2012).
10. Yum, J.-H. *et al.* A cobalt complex redox shuttle for dye-sensitized solar cells with high open-circuit potentials. *Nat. Commun.* **3**, 631 (2012).
11. Meyer, G. J. The 2010 Millennium Technology Grand Prize: Dye-Sensitized Solar Cells. *ACS Nano* **4**, 4337–4343 (2010).
12. Green, M. A., Emery, K., Hishikawa, Y., Warta, W. & Dunlop, E. D. Solar cell efficiency tables (version 39). *Prog. Photovoltaics* **20**, 12–20 (2012).
13. Alex, S., Santhosh, U. & Das, S. Dye sensitization of nanocrystalline TiO_2: enhanced efficiency of unsymmetrical versus symmetrical squaraine dyes. *J. Photochem. Photobiol. A* **172**, 63–71 (2005).
14. Li, C., Wang, W., Wang, X. S., Zhang, B. W. & Cao, Y. Molecular design of squaraine dyes for efficient far-red and near-IR sensitization of solar cells. *Chem. Lett.* **34**, 554–555 (2005).
15. Burke, A., Schmidt-Mende, L., Ito, S. & Grätzel, M. A novel blue dye for near-IR 'dye-sensitised' solar cell applications. *Chem. Commun.* 234–236 (2007).
16. Yum, J.-H. *et al.* Efficient far red sensitization of nanocrystalline TiO_2 films by an unsymmetrical squaraine dye. *J. Am. Chem. Soc.* **129**, 10320–10321 (2007).
17. Geiger, T. *et al.* Molecular design of unsymmetrical squaraine dyes for high efficiency conversion of low energy photons into electrons using TiO_2 nanocrystalline films. *Adv. Funct. Mater.* **19**, 2720–2727 (2009).
18. Park, J. *et al.* Symmetric vs. asymmetric squaraines as photosensitisers in mesoscopic injection solar cells: a structure-property relationship study. *Chem. Commun.* **48**, 2782–2784 (2012).
19. Shi, Y. *et al.* A high-efficiency panchromatic squaraine sensitizer for dye-sensitized solar cells. *Angew. Chem. Inter. Ed.* **50**, 6619–6621 (2011).
20. Delcamp, J. H. *et al.* The Role of pi Bridges in High-Efficiency DSCs Based on Unsymmetrical Squaraines. *Chem-Eur. J.* **19**, 1819–1827 (2013).
21. Hao, Z. M. & Iqbal, A. Some aspects of organic pigments. *Chem. Soc. Rev.* **26**, 203–213 (1997).
22. Beaujuge, P. M. & Frechet, J. M. J. Molecular Design and Ordering Effects in pi-Functional Materials for Transistor and Solar Cell Applications. *J. Am. Chem. Soc.* **133**, 20009–20029 (2011).
23. Nielsen, C. B., Turbiez, M. & McCulloch, I. Recent Advances in the Development of Semiconducting DPP-Containing Polymers for Transistor Applications. *Adv. Mater.* **25**, 1859–1880 (2013).
24. Kanimozhi, C., Balraju, P., Sharma, G. D. & Patil, S. Diketopyrrolopyrrole-Based Donor-Acceptor Copolymers as Organic Sensitizers for Dye Sensitized Solar Cells. *J. Phys. Chem. C* **114**, 3287–3291 (2010).
25. Qu, S. Y. *et al.* New Diketopyrrolopyrrole (DPP) Dyes for Efficient Dye-Sensitized Solar Cells. *J. Phys. Chem. C* **114**, 1343–1349 (2010).
26. Warnan, J. *et al.* A compact diketopyrrolopyrrole dye as efficient sensitizer in titanium dioxide dye-sensitized solar cells. *J. Photochem. Photobiol. A* **226**, 9–15 (2011).
27. Qu, S. Y. *et al.* A novel D-A-pi-A organic sensitizer containing a diketopyrrolopyrrole unit with a branched alkyl chain for highly efficient and stable dye-sensitized solar cells. *Chem. Commun.* **48**, 6972–6974 (2012).
28. Qu, S. Y. *et al.* New diketo-pyrrolo-pyrrole (DPP) sensitizer containing a furan moiety for efficient and stable dye-sensitized solar cells. *Dyes Pigments* **92**, 1384–1393 (2012).
29. Zhang, F. *et al.* A novel compact DPP dye with enhanced light harvesting and charge transfer properties for highly efficient DSCs. *J. Mater. Chem. A* **1**, 4858–4863 (2013).
30. Holcombe, T. W. *et al.* A structural study of DPP-based sensitizers for DSC applications. *Chem. Commun.* **48**, 10724–10726 (2012).
31. Yum, J.-H. *et al.* Towards high-performance DPP-based sensitizers for DSC applications. *Chem. Commun.* **48**, 10727–10729 (2012).
32. Kaduk, B., Kowalczyk, T. & Van Voorhis, T. Constrained Density Functional Theory. *Chem. Rev.* **112**, 321–370 (2011).
33. Kantchev, E. A. B., Norsten, T. B. & Sullivan, M. B. Time-dependent density functional theory (TDDFT) modelling of Pechmann dyes: from accurate absorption maximum prediction to virtual dye screening. *Org. Biomol. Chem.* **10**, 6682–6692 (2012).
34. Boese, A. D. & Martin, J. M. L. Development of density functionals for thermochemical kinetics. *J. Chem. Phys.* **121**, 3405–3416 (2004).
35. Zhao, Y. & Truhlar, D. G. Density Functionals with Broad Applicability in Chemistry. *Acc. Chem. Res.* **41**, 157–167 (2008).
36. Marenich, A. V., Cramer, C. J. & Truhlar, D. G. Universal Solvation Model Based on Solute Electron Density and on a Continuum Model of the Solvent Defined by the Bulk Dielectric Constant and Atomic Surface Tensions. *J. Phys. Chem. B* **113**, 6378–6396 (2009).
37. Godbout, N., Salahub, D. R., Andzelm, J. & Wimmer, E. Optimization of Gaussian-Type Basis-Sets for Local Spin-Density Functional Calculations .1. Boron through Neon, Optimization Technique and Validation. *Can. J. Chem.* **70**, 560–571 (1992).
38. Sosa, C. *et al.* A Local Density Functional-Study of the Structure and Vibrational Frequencies of Molecular Transition-Metal Compounds. *J. Phys. Chem.* **96**, 6630–6636 (1992).
39. Connelly, N. G. & Geiger, W. E. Chemical redox agents for organometallic chemistry. *Chem. Rev.* **96**, 877–910 (1996).
40. Sapp, S. A., Elliott, C. M., Contado, C., Caramori, S. & Bignozzi, C. A. Substituted polypyridine complexes of cobalt(II/III) as efficient electron-transfer mediators in dye-sensitized solar cells. *J. Am. Chem. Soc.* **124**, 11215–11222 (2002).
41. Kavan, L., Yum, J.-H. & Grätzel, M. Graphene Nanoplatelets Outperforming Platinum as the Electrocatalyst in Co-Bipyridine-Mediated Dye-Sensitized Solar Cells. *Nano Lett.* **11**, 5501–5506 (2011).
42. Kavan, L., Yum, J.-H., Nazeeruddin, M. K. & Grätzel, M. Graphene Nanoplatelet Cathode for Co(III)/(II) Mediated Dye-Sensitized Solar Cells. *Acs Nano* **5**, 9171–9178 (2011).
43. Zhang, Z. P., Ito, S., Moser, J. E., Zakeeruddin, S. M. & Grätzel, M. Influence of Iodide Concentration on the Efficiency and Stability of Dye-Sensitized Solar Cell Containing Non-Volatile Electrolyte. *Chemphyschem* **10**, 1834–1838 (2009).
44. Roy-Mayhew, J. D., Bozym, D. J., Punckt, C. & Aksay, I. A. Functionalized Graphene as a Catalytic Counter Electrode in Dye-Sensitized Solar Cells. *ACS Nano* **4**, 6203–6211 (2010).
45. Fabregat-Santiago, F. *et al.* Correlation between photovoltaic performance and impedance spectroscopy of dye-sensitized solar cells based on ionic liquids. *J. Phys. Chem. C* **111**, 6550–6560 (2007).
46. O'Regan, B. C. & Lenzmann, F. Charge transport and recombination in a nanoscale interpenetrating network of n-type and p-type semiconductors:

Transient photocurrent and photovoltage studies of TiO_2/Dye/CuSCN photovoltaic cells. *J. Phys. Chem. B* **108**, 4342–4350 (2004).
47. Fabregat-Santiago, F., Bisquert, J., Garcia-Belmonte, G., Boschloo, G. & Hagfeldt, A. Influence of electrolyte in transport and recombination in dye-sensitized solar cells studied by impedance spectroscopy. *Sol. Energy Mater. Sol. Cells* **87**, 117–131 (2005).

Acknowledgments

We acknowledge the joint development project funded by Dongjin Semichem Co., Ltd. (S. Korea), the European Research Council (ERC) for an Advanced Research Grant (ARG 247404) funded under the "Mesolight" project, and the European Community's Seventh Framework Programme (FP7/2007–2013) under grant agreement no. 246124 of the SANS project. The authors thank Prof. J.-E. Moser for providing access to the TAS facility and Mr. Pascal Comte, Dr. Yella Aswani, and Dr. Florian Kessler for their kind assistance in preparing the TiO_2 paste, the carbonaceous catalyst solution and the cobalt complexes.

Author contributions

J.H.Y., T.W.H. and M.G. conceived the experiment. T.W.H., J.H.D. and K.R. synthesized the donors; T.W.H. and K.R. synthesized the sensitizers. J.H.Y. and Y.J.K. performed the photovoltaic experiments and photophysical and electrochemical experiments for the sensitizers. J.H.Y. and T.M. performed the EIS experiments and J.T. performed the time resolved nanosecond laser spectroscopy. All the authors participated in discussions of the research.

Additional information

Supplementary information accompanies this paper at http://www.nature.com/scientificreports

Competing financial interests: The authors declare no competing financial interests.

How to cite this article: Yum, J.-H. *et al.* Blue-Coloured Highly Efficient Dye-Sensitized Solar Cells by Implementing the Diketopyrrolopyrrole Chromophore. *Sci. Rep.* **3**, 2446; DOI:10.1038/srep02446 (2013).